Available online at www.sciencedirect.com
ScienceDirect
Journal of Sound and Vibration 298 (2006) 206–220
JOURNAL OF SOUND AND VIBRATION
www.elsevier.com/locate/jsvi

Topology design optimization of structures at high frequencies using power flow analysis

Seonho Cho, Chan-Young Park, Young-Ho Park, Suk-Yoon Hong*

Department of Naval Architecture and Ocean Engineering, Research Institute of Marine and Systems Engineering (RIMSE), Seoul National University, San 56-1, Sillim-Dong, Kwanak-Gu, Seoul, South Korea

Received 27 August 2004; received in revised form 3 April 2006; accepted 11 May 2006
Available online 10 July 2006

Abstract

A density–based topology optimization method is developed for power flow problems in steady state using an adjoint design sensitivity analysis (DSA) method. Design variables such as Young's modulus, density, and damping factor are parameterized using a bulk material density function. A generalized compliance of structures, defined as the inner product of prescribed loading and response function, is selected as an objective function. The objective is to minimize the generalized compliance within allowable material volume. Since already factorized system matrix obtained from the power flow analysis is utilized to evaluate the adjoint response and sensitivity, computational cost for the DSA is trivial. Through several numerical examples, the developed DSA method is verified to yield very accurate sensitivity, requiring only 0.15% of CPU cost for finite difference sensitivity. Also, it turns out that the developed method can yield an optimal structural layout to transmit the vibrational power effectively.

1. Introduction

For the dynamic analysis of structural systems in high frequency ranges, the finite-element method (FEM) and boundary element method (BEM) to obtain the kinematic responses are not suitable due to mesh size requirement that is closely related to the quality of analysis. Moreover, at high frequencies, the uncertainty of system parameters gets increased and consequently the quality of analysis results becomes worse. Therefore, it is desirable to employ the statistical methods that predict the modal- and frequency-averaged vibrational behavior of systems. The statistical energy analysis (SEA) is one of the methods developed to overcome the difficulties in high frequency ranges. However, the SEA is well suited only for high-frequency problems with high modal density. Also, it fails to provide the spatial information of energy distribution. As an alternative, a flow analysis (PFA) method regards "flow of vibrational energy" as "flow of heat" in thermal systems. Similar to the thermal problems, the governing equation for the PFA is a parabolic partial differential equation. The PFA which is originally devised by Belov et al. [1] enables to predict the spatial energy variation in structures. Butlitskaya et al. [2] used the energy equation developed by Belov et al. to investigate the propagation of both

*Corresponding author. Tel.: +82 2 880 8757; fax: +82 2 888 9298.
E-mail address: syh@snu.ac.kr (S.-Y. Hong).

0022-460X/$ - see front matter © 2006 Elsevier Ltd. All rights reserved.
doi:10.1016/j.jsv.2006.05.015

vibrational and acoustic energy in structures. Cremer et al. [3] showed that in an elastic medium, the time-averaged dissipated power at a point is proportional to the time averaged potential energy density at that point. Nefske and Sung [4] developed the equations which govern the flow of energy in homogeneous finite beams and implemented the finite-element analysis of vibrational energy equation. Lase and Jezequel [5] derive an equation which governs the spatially harmonic component of the energy density in rods. Bouthier and Bernhard [6,7] derived for propagation of flexural waves and thus, a single plate can be analyzed with the power flow analysis using space–time averaged potential energy density. Using a loss factor damping model, the simplified models of energy distribution in membranes and transversely vibrating plates at high frequencies are derived. Power flow finite element method (PFFEM) is used to obtain the vibrational response of plates excited by point harmonic forces. The relation between dynamic problem and power flow problem and loading and boundary conditions are well discussed in Refs. [6–9].

A topology optimization method enables designers to find a suitable material layout for the required performances of systems. For instance, in solid mechanics problems, the objective function and constraint are the compliance and material volume of system, respectively. The material property in each element is selected as the design variable. The objective of topology optimization is to find an optimal material layout within the allowed material volume by varying the material property of each element. Ever since Bendsøe and Kikuchi [10] introduced the topology optimization method using a homogenization approach, many topology optimization methods have been developed for both linear and nonlinear structural problems in many disciplines such as solid mechanics, thermal, eigenvalue, and acoustic problems. Nowadays, the density method [11] is preferred due to its simple implementation compared with the homogenization method. The density method defines a bulk material density, regarded as the design variables varying from zero (void state) to unity (solid state), to distribute the material in the continuum design domain. Unfortunately, there is little literature regarding the topology optimization of power flow problems. For the similar problem that is analogous to the power flow problem, Li et al. [12] performed a topology optimization of heat conduction problems using evolutionary structural optimization method.

Since the topology optimization necessarily involves many design variables, the sensitivity of performance measures with respect to the design variables should be determined in a very efficient way. The DSA method computes the variation of the structural response with respect to design variables [13]. In continuum approach, the design sensitivity expressions are obtained by taking the first-order variation of continuum variational equation that represents the structural system. Among various DSA methods, the adjoint variable method is computationally efficient especially for the problems that have many design variables but small number of performance measures because their design sensitivity can be computed in a selective manner. Thus, the adjoint DSA method is widely used in the topology optimization problems. In this paper, a continuum method for the non-shape problems like material property DSA is considered for the PFA in steady state. Kim et al. [14] derived the continuum-based design sensitivity expressions for the general PFA problems. As similar studies on the heat conduction problems, Tortorelli et al. derived the shape design sensitivity for nonlinear transient thermal systems using the Lagrange multiplier method [15] and the adjoint method [16]. Sluzalec and Kleiber [17] employed the Kirchhoff transformation to derive the shape design sensitivity expressions for linearized heat conduction problems using the adjoint variable approach.

In Section 2, the governing equation and weak formulation for the PFA are briefly reviewed. In Section 3, the direct differentiation and adjoint methods are discussed to formulate a continuum-based DSA method. In Section 4, a design parameterization method is discussed and the topology optimization of power flow problems is formulated using the adjoint sensitivity and a gradient-based optimization method. In Section 5, some numerical examples are demonstrated to verify the accuracy and efficiency of the developed analytical DSA method compared with finite difference sensitivity. Also, the topology design optimization is performed to verify the applicability of the developed method for several power flow problems.

2. Review of power flow analysis

Consider a structural body occupying an open domain Ω bounded by a closed surface Γ as shown in Fig. 1. All the material properties are assumed homogeneous and isotropic in the domain Ω. Boundaries are

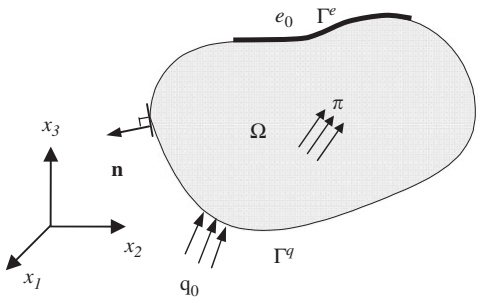

Fig. 1. Structural body in space.

composed of an energy (essential) boundary Γ^e and a flux (natural) boundary Γ^q such that $\Gamma^e \cup \Gamma^q$ and $\Gamma^e \cap \Gamma^q = \phi$.

A governing equation for power flow problems in steady state is written by

$$-\frac{c_g^2}{\eta\omega}\nabla^2 e + \eta\omega e = \pi, \tag{1}$$

where e, η, ω, π , and c_g are the time- and space-averaged energy density function, hysteresis damping factor, excitation frequency, the rate of internal energy generation, and group velocity, respectively. For plate structures, the group velocity is defined by

$$\begin{aligned} c_g &= 2 \times \sqrt[4]{\frac{\omega^2 D}{\rho h}}, \\ &= 2 \times \sqrt[4]{\frac{\omega^2 E h^2}{12\rho(1-\nu^2)}}, \end{aligned} \tag{2}$$

where ρ, ν, h, E, and D are the density, Poisson's ratio, thickness, Young's modulus, and flexural rigidity of plate, respectively. A prescribed energy e_0 on Γ^e and a prescribed flux q_0 on Γ^q in the inward normal direction are imposed as

$$e = e_0 \text{ on } \Gamma^e \tag{3}$$

and

$$q = q_0 \text{ on } \Gamma^q \tag{4}$$

The d-dimensional space Z for the trial solution is defined as

$$Z = \{e \in \left[H^1(\Omega)\right]^d : e = e_0 \text{ on } \Gamma^e\} \tag{5}$$

and $\bar{Z}$ for the virtual field as

$$\bar{Z} = \{\bar{e} \in \left[H^1(\Omega)\right]^d : \bar{e} = 0 \text{ on } \Gamma^e\}. \tag{6}$$

Using the virtual field $\bar{e}$, the weak form of Eq. (1) is written as

$$\int_{\Omega\Gamma}\left(-\frac{c_g^2}{\eta\omega}\nabla^2 e\bar{e} + \eta\omega e\bar{e}\right)\mathrm{d}\Omega = \int_{\Omega}\pi\bar{e}\,\mathrm{d}\Omega \text{ for all } \bar{e} \in \bar{Z}. \tag{7}$$

Using the divergence theorem and Eq. (3), Eq. (7) can be rewritten as

$$\int_{\Omega}\left(\frac{c_g^2}{\eta\omega}\nabla e \cdot \nabla\bar{e}\right)\mathrm{d}\Omega + \int_{\Omega}(\eta\omega e\bar{e})\,\mathrm{d}\Omega = \int_{\Omega}\pi\bar{e}\,\mathrm{d}\Omega - \int_{\Gamma^q}\left(-\frac{c_g^2}{\eta\omega}\nabla e\right)\cdot\mathbf{n}\bar{e}\,\mathrm{d}\Gamma \text{ for all } \bar{e} \in \bar{Z}. \tag{8}$$

Defining a time-and space-averaged intensity $\mathbf{I}$ as

$$\mathbf{I} = -\frac{c_g^2}{\eta\omega}\nabla e \tag{9}$$

and a flux q as

$$q = \mathbf{I}\cdot\mathbf{n}. \tag{10}$$

Eq. (8) is reduced to

$$\int_\Omega \left(\frac{c_g^2}{\eta\omega}\nabla e\cdot\nabla\bar{e} + \eta\omega e\bar{e}\right)\mathrm{d}\Omega = \int_\Omega \pi\bar{e}\,\mathrm{d}\Omega - \int_{\Gamma^q} q\bar{e}\,\mathrm{d}\Gamma \text{ for all } \bar{e}\in\bar{Z}. \tag{11}$$

Defining a bilinear form

$$a(e,\bar{e}) \equiv \int_\Omega \left(\frac{c_g^2}{\eta\omega}\nabla e\cdot\nabla\bar{e} + \eta\omega e\bar{e}\right)\mathrm{d}\Omega \tag{12}$$

and a linear form

$$\ell(\bar{e}) \equiv \int_\Omega \pi\bar{e}\,\mathrm{d}\Omega - \int_{\Gamma^q} q\bar{e}\,\mathrm{d}\Gamma. \tag{13}$$

Eq. (11) can be rewritten, in abstract form, as

$$a(e,\bar{e}) = \ell(\bar{e}) \text{ for all } \bar{e}\in\bar{Z}. \tag{14}$$

3. Continuum-based design sensitivity analysis

3.1. Direct differentiation method (DDM)

For the given design $\mathbf{u}$, Eq. (14) can be rewritten as

$$a_{\mathbf{u}}(e,\bar{e}) = \ell_{\mathbf{u}}(\bar{e}) \text{ for all } \bar{e}\in\bar{Z}, \tag{15}$$

where the subscript $\mathbf{u}$ indicates the dependence of the abstract form on the design variations. The variational equation corresponding to the perturbed design $\mathbf{u}+\tau\delta\mathbf{u}$ is written as

$$a_{\mathbf{u}+\tau\delta\mathbf{u}}(e_\tau,\bar{e}) = \ell_{\mathbf{u}+\tau\delta\mathbf{u}}(\bar{e}) \text{ for all } \bar{e}\in\bar{Z}. \tag{16}$$

The first-order variations of each term in Eq. (15) with respect to its explicit dependence on the design variable $\mathbf{u}$ are defined as

$$a'_{\delta\mathbf{u}}(e,\bar{e}) \equiv \frac{\mathrm{d}}{\mathrm{d}\tau}a_{\mathbf{u}+\tau\delta\mathbf{u}}(\tilde{e}_\tau,\bar{e})\bigg|_{\tau=0} \tag{17}$$

and

$$\ell'_{\delta\mathbf{u}}(\bar{e}) \equiv \frac{\mathrm{d}}{\mathrm{d}\tau}\ell_{\mathbf{u}+\tau\delta\mathbf{u}}(\bar{e})\bigg|_{\tau=0}, \tag{18}$$

where the '$\sim$' denotes that the dependence on design variations is suppressed. Note that $\bar{e}$ is independent of τ. Define the first-order variation of the solution of Eq. (15) as

$$e' \equiv \frac{\mathrm{d}}{\mathrm{d}\tau}e(\mathbf{u}+\tau\delta\mathbf{u})\bigg|_{\tau=0} = \lim_{\tau\to0}\frac{e(\mathbf{u}+\tau\delta\mathbf{u})-e(\mathbf{u})}{\tau}. \tag{19}$$

Using the chain rule of differentiation and Eq. (17), the following holds

$$\frac{\mathrm{d}}{\mathrm{d}\tau}[a_{\mathbf{u}+\tau\delta\mathbf{u}}(e(\mathbf{u}+\tau\delta\mathbf{u}),\bar{e})]\bigg|_{\tau=0} = a'_{\delta\mathbf{u}}(e,\bar{e}) + a_{\mathbf{u}}(e',\bar{e}). \tag{20}$$

Using Eqs. (18) and (20) and taking the first-order variation of Eq. (15) lead to

$$a_{\mathbf{u}}(e', \bar{e}) = \ell'_{\delta\mathbf{u}}(\bar{e}) - a'_{\delta\mathbf{u}}(e, \bar{e}) \text{ for all } \bar{e} \in \bar{Z}. \tag{21}$$

Next, consider a general performance functional that may be written, in integral forms, as

$$\psi = \int_{\Omega} g_1(\mathbf{u}, e, \nabla e)\, \mathrm{d}\Omega + \int_{\Gamma} g_2(\mathbf{u}, e, \nabla e)\, \mathrm{d}\Gamma. \tag{22}$$

Taking the first-order variation of Eq. (22), one has the following expression.

$$\begin{aligned}\psi' &= \frac{\mathrm{d}}{\mathrm{d}\tau}\left[\int_{\Omega} g_1\{\mathbf{u}+\tau\delta\mathbf{u}, e(\mathbf{u}+\tau\delta\mathbf{u}), \nabla e(\mathbf{u}+\tau\delta\mathbf{u})\}\, \mathrm{d}\Omega + \int_{\Gamma} g_2\{\mathbf{u}+\tau\delta\mathbf{u}, e(\mathbf{u}+\tau\delta\mathbf{u}), \nabla e(\mathbf{u}+\tau\delta\mathbf{u})\}\, \mathrm{d}\Gamma\right]\Bigg|_{\tau=0} \\ &= \int_{\Omega} \left(g_{1,\mathbf{u}}\delta\mathbf{u} + g_{1,e}e' + g_{1,\nabla e}\nabla e'\right) \mathrm{d}\Omega + \int_{\Gamma} \left(g_{2,\mathbf{u}}\delta\mathbf{u} + g_{2,e}e' + g_{2,\nabla e}\nabla e'\right) \mathrm{d}\Gamma. \end{aligned} \tag{23}$$

Once finding e' from Eq. (21), one trivially obtains the design sensitivity of performance measure from Eq. (23).

3.2. Adjoint variable method

First of all, define an adjoint equation for the power flow problems. Replace the implicit dependence terms in Eq. (23) by a virtual energy density $\bar{\lambda}$ and equate the terms involving $\bar{\lambda}$ to the bilinear form $a_{\mathbf{u}}(\lambda, \bar{\lambda})$ to yield the adjoint equation as

$$a_{\mathbf{u}}(\lambda, \bar{\lambda}) = \int_{\Omega} \left(g_{1,e}\bar{\lambda} + g_{1,\nabla e}\nabla\bar{\lambda}\right) \mathrm{d}\Omega + \int_{\Gamma} \left(g_{2,e}\bar{\lambda} + g_{2,\nabla e}\nabla\bar{\lambda}\right) \mathrm{d}\Gamma \text{ for all } \bar{\lambda} \in \bar{Z}, \tag{24}$$

where the adjoint response λ satisfies the homogeneous boundary conditions. Since $\bar{e} \in \bar{Z}$ and $\lambda \in \bar{Z}$, Eq. (21) can be rewritten as

$$a_{\mathbf{u}}(e', \lambda) = \ell'_{\delta\mathbf{u}}(\lambda) - a'_{\delta\mathbf{u}}(e, \lambda) \text{ for all } \lambda \in \bar{Z}. \tag{25}$$

Since $e' \in \bar{Z}$, Eq. (24) can be rewritten as

$$a_{\mathbf{u}}(\lambda, e') = \int_{\Omega} \left(g_{1,e}e' + g_{1,\nabla e}\nabla e'\right) \mathrm{d}\Omega + \int_{\Gamma} \left(g_{2,e}e' + g_{2,\nabla e}\nabla e'\right) \mathrm{d}\Gamma \text{ for all } e' \in \bar{Z}. \tag{26}$$

Now that $a_{\mathbf{u}}(\bullet, \bullet)$ is a symmetric operator, the following holds:

$$a_{\mathbf{u}}(e', \lambda) = a_{\mathbf{u}}(\lambda, e'). \tag{27}$$

Eqs. (25) and (26) are equivalent so that one can write the following equation:

$$\int_{\Omega} \left(g_{1,e}e' + g_{1,\nabla e}\nabla e'\right) \mathrm{d}\Omega + \int_{\Gamma} \left(g_{2,e}e' + g_{2,\nabla e}\nabla e'\right) \mathrm{d}\Gamma = \ell'_{\delta\mathbf{u}}(\lambda) - a'_{\delta\mathbf{u}}(e, \lambda). \tag{28}$$

Substituting Eq. (28) into Eq. (23), one finally obtains

$$\psi' = \int_{\Omega} g_{1,\mathbf{u}}\delta\mathbf{u}\, \mathrm{d}\Omega + \int_{\Gamma} g_{2,\mathbf{u}}\delta\mathbf{u}\, \mathrm{d}\Gamma + \ell'_{\delta\mathbf{u}}(\lambda) - a'_{\delta\mathbf{u}}(e, \lambda). \tag{29}$$

To evaluate Eq. (29), one needs not only the original response e but also adjoint response λ. The efficiency and accuracy of Eq. (29) will be demonstrated in section 5.

4. Formulation of topology design optimization

The objective of topology optimization method is to find an optimal material distribution that minimizes the energy stored in the system under prescribed loadings. The material distribution can be represented using a normalized bulk material density function u that has a continuous variation from zero to one, taking the value of 1.0 for solid material and 0.0 for void. For the topology optimization using the FEM, the structural domain is discretized into NE finite elements. The bulk material density is assumed constant in each element.

The material properties involved in the power flow analysis are the Young's modulus E, Poisson's ratio v, hysteresis damping factor η, and density ρ, as shown in the following expression derived from Eqs. (1) and (2).

$$\begin{aligned}\pi &= -\frac{c_g^2}{\eta\omega}\nabla^2 e + \eta\omega e \\ &= -2\sqrt{\frac{\omega^2 E h^2}{3\rho(1-v^2)}}\frac{\nabla^2 e}{\eta\omega} + \eta\omega e. \end{aligned} \tag{30}$$

Through parametric studies, it turns out that the variation of Poisson's ratio affects little impact on the performance of systems. The design variable that is the bulk material density of each element is associated with the Young's modulus, hysteresis damping factor, and density as

$$E_i = u_i^p E_0, \tag{31}$$

$$\eta_i = u_i^r \eta_0, \tag{32}$$

and

$$\rho_i = u_i^s \rho_0, \tag{33}$$

where

$$0 < u_{\min} \le u_i \le 1, \quad (i = 1, 2, \ldots, \mathrm{NE}). \tag{34}$$

E_0, η_0, ρ_0 denote the original material properties. p, r, and s are the penalty parameters used to enforce the concentrated distribution of material volume. The lower bound of material, $u_{\min}$, is introduced to avoid numerical singularity. Substituting the continuous form of Eqs. (31)–(33) into Eq. (30), one obtains the following expression:

$$\pi = -2u^{(p-2r-s)/2}\sqrt{\frac{\omega^2 E_0 h^2}{3\rho_0(1-v^2)}}\frac{\nabla^2 e}{\eta_0\omega} + u^r\eta_0\omega e. \tag{35}$$

Note that the numerous combinations of penalty parameters are possible depending on the assumption about the material parameterization model. If one makes an assumption that the first and second terms in Eq. (35) have the same contribution on the governing equation as the bulk material density varies, the condition for parameters is derived as

$$p - 4r - s = 0. \tag{36}$$

Using the aforementioned density approach, a topology optimization problem is stated as

$$\text{Minimize } \Pi = \int_\Omega \pi e \,\mathrm{d}\Omega - \int_{\Gamma^q} qe \,\mathrm{d}\Gamma, \tag{37}$$

$$\text{Subject to } \int_\Omega u \,\mathrm{d}\Omega \le V_{\text{allowable}}, \tag{38}$$

where $\prod$ and $V_{\text{allowable}}$ are a so called "generalized compliance" and an allowable volume, respectively. The notion of generalized compliance in the power flow problems is extended from the well-known structural compliance that is the inner product of external load and displacement field. The physical meaning of minimization of generalized compliance is to find a material layout that stores minimal energy density for the prescribed external loadings. For the required sensitivity of objective function, one has the adjoint sensitivity expression for the generalized compliance functional, using Eq. (29), as

$$\begin{aligned}\psi' &= \int_\Omega g_{1,\mathbf{u}}\delta\mathbf{u}\,\mathrm{d}\Omega + \int_\Gamma g_{2,\mathbf{u}}\delta\mathbf{u}\,\mathrm{d}\Gamma + \ell'_{\delta\mathbf{u}}(\lambda) - a'_{\delta\mathbf{u}}(e,\lambda) \\ &= -\int_\Omega \left(\frac{2c_g c_g'\eta - c_g^2\eta'}{\eta^2\omega}\nabla e\cdot\nabla\lambda + \eta'\omega e\lambda\right)\mathrm{d}\Omega. \end{aligned} \tag{39}$$

The adjoint equation is written, using Eq. (37), as

$$a_{\mathbf{u}}(\lambda,\bar{\lambda}) = \int_{\Omega} \pi\bar{\lambda}\,\mathrm{d}\Omega - \int_{\Gamma^q} q\bar{\lambda}\,\mathrm{d}\Gamma \ \text{ for all } \ \bar{\lambda} \in \bar{Z}. \tag{40}$$

Comparing Eq. (40) with Eq. (11), the following holds since $\bar{\lambda}, \bar{e} \in \bar{Z}$:

$$\lambda = e. \tag{41}$$

Thus, Eq. (39) can be finally written as

$$\psi' = -\int_{\Omega} \left(\frac{2c_g c_g' \eta - c_g^2 \eta'}{\eta^2 \omega} \nabla e \cdot \nabla e + \eta' \omega e e \right) \mathrm{d}\Omega. \tag{42}$$

For the topology optimization, it is very important to make the problem convex to obtain a unique optimal solution regardless of initial design. Otherwise, it may have many local minima and thus the optimal result depends on its initial design significantly. If the Hessian of the unconstrained function composed of objective function and constraints is positive definite, the optimization problem is convex. In this topology optimization formulation, only linear constraints with respect to the design variables are considered so that the Hessian of objective function affects the convexity of problem. Consider a state equation in matrix form, which is equivalent to Eq. (14) as

$$\begin{aligned} \mathbf{t}[\mathbf{u}, e(\mathbf{u})] &= \mathbf{f}_{\text{int}} - \mathbf{f}_{\text{ext}} \\ &= \mathbf{K}\mathbf{e} - \mathbf{f}_{\text{ext}} = \mathbf{0}, \end{aligned} \tag{43}$$

where $\mathbf{f}_{\text{int}}$, $\mathbf{f}_{\text{ext}}$, $\mathbf{K}$, and $\mathbf{e}$ are the internal load, external load, system matrix, and the response vector that is the energy density function, respectively. Taking derivative of Eq. (43) with respect to the response $\mathbf{e}$ leads to

$$\frac{\partial \mathbf{t}}{\partial \mathbf{e}} = \mathbf{K}. \tag{44}$$

Also taking derivative of Eq. (43) with respect to the design variable $\mathbf{u}$ yields

$$\frac{\mathrm{d}\mathbf{t}}{\mathrm{d}\mathbf{u}} = \frac{\partial \mathbf{t}}{\partial \mathbf{u}} + \frac{\partial \mathbf{t}}{\partial \mathbf{e}} \frac{\mathrm{d}\mathbf{e}}{\mathrm{d}\mathbf{u}} = 0 \tag{45}$$

or

$$\frac{\mathrm{d}\mathbf{e}}{\mathrm{d}\mathbf{u}} = -\mathbf{K}^{-1} \frac{\partial \mathbf{t}}{\partial \mathbf{u}}. \tag{46}$$

Taking derivative of Eq. (43) with respect to the design variable $\mathbf{u}$ yields

$$\frac{\mathrm{d}\mathbf{K}}{\mathrm{d}\mathbf{u}}\mathbf{e} + \mathbf{K}\frac{\mathrm{d}\mathbf{e}}{\mathrm{d}\mathbf{u}} = 0. \tag{47}$$

Substituting Eq. (46) into Eq. (47) yields

$$\frac{\partial \mathbf{t}}{\partial \mathbf{u}} = \frac{\mathrm{d}\mathbf{K}}{\mathrm{d}\mathbf{u}}\mathbf{e}. \tag{48}$$

In the power flow problems, the generalized compliance functional is defined by

$$\prod = \int_{\Omega} \pi e\,\mathrm{d}\Omega - \int_{\Gamma^q} qe\,\mathrm{d}\Gamma = \frac{1}{2}\int_{\Omega} \left(\frac{c_g^2}{\eta\omega} \nabla e \cdot \nabla e + \eta\omega e e \right) \mathrm{d}\Omega$$

or

$$\Pi = \mathbf{f}_{\text{ext}}^{\mathrm{T}}\mathbf{e} = \frac{1}{2}\mathbf{e}^{\mathrm{T}}\mathbf{K}\mathbf{e}. \tag{49}$$

Taking derivative of the compliance functional with respect to the design variable $\mathbf{u}$ leads to

$$\frac{d\Pi}{d\mathbf{u}} = \mathbf{e}^T\mathbf{K}\left(\frac{d\mathbf{e}}{d\mathbf{u}}\right) + \frac{1}{2}\mathbf{e}^T\frac{d\mathbf{K}}{d\mathbf{u}}\mathbf{e}. \tag{50}$$

Using Eqs. (46) and (48), Eq. (50) can be rewritten as

$$\frac{d\Pi}{d\mathbf{u}} = -\frac{1}{2}\mathbf{e}^T\left(\frac{\partial\mathbf{t}}{\partial\mathbf{u}}\right). \tag{51}$$

Taking derivative of Eq. (51) again with respect to the design variable $\mathbf{u}$ yields

$$\frac{d^2\Pi}{d\mathbf{u}^2} = -\frac{1}{2}\left(\frac{d\mathbf{e}}{d\mathbf{u}}\right)^T\left(\frac{\partial\mathbf{t}}{\partial\mathbf{u}}\right) - \frac{1}{2}\mathbf{e}^T\frac{d}{d\mathbf{u}}\left(\frac{\partial\mathbf{t}}{\partial\mathbf{u}}\right). \tag{52}$$

Using Eqs. (46) and (48), Eq. (52) can be rewritten as

$$\frac{d^2\Pi}{d\mathbf{u}^2} = \frac{1}{2}\left(\frac{\partial\mathbf{t}}{\partial\mathbf{u}}\right)^T\mathbf{K}^{-1}\left(\frac{\partial\mathbf{t}}{\partial\mathbf{u}}\right) - \frac{1}{2}\mathbf{e}^T\frac{d}{d\mathbf{u}}\left(\frac{d\mathbf{K}}{d\mathbf{u}}\mathbf{e}\right). \tag{53}$$

The last term of Eq. (53) is rewritten as

$$-\frac{1}{2}\mathbf{e}^T\frac{d}{d\mathbf{u}}\left(\frac{d\mathbf{K}}{d\mathbf{u}}\mathbf{e}\right) = -\frac{1}{2}\mathbf{e}^T\frac{d^2\mathbf{K}}{d\mathbf{u}^2}\mathbf{e} - \frac{1}{2}\mathbf{e}^T\frac{d\mathbf{K}}{d\mathbf{u}}\frac{d\mathbf{e}}{d\mathbf{u}}. \tag{54}$$

Using Eqs. (46) and (48), Eq. (54) can be rewritten as

$$-\frac{1}{2}\mathbf{e}^T\frac{d}{d\mathbf{u}}\left(\frac{d\mathbf{K}}{d\mathbf{u}}\mathbf{e}\right) = -\frac{1}{2}\mathbf{e}^T\frac{d^2\mathbf{K}}{d\mathbf{u}^2}\mathbf{e} + \frac{1}{2}\left(\frac{\partial\mathbf{t}}{\partial\mathbf{u}}\right)^T\mathbf{K}^{-1}\left(\frac{\partial\mathbf{t}}{\partial\mathbf{u}}\right). \tag{55}$$

Thus, Eq. (53) is rewritten as

$$\frac{d^2\Pi}{d\mathbf{u}^2} = \left(\frac{\partial\mathbf{t}}{\partial\mathbf{u}}\right)^T\mathbf{K}^{-1}\left(\frac{\partial\mathbf{t}}{\partial\mathbf{u}}\right) - \frac{1}{2}\mathbf{e}^T\frac{d^2\mathbf{K}}{d\mathbf{u}^2}\mathbf{e}. \tag{56}$$

Assuming that the parameters obey the rule in Eq. (36), Eq. (35) is rewritten as

$$\pi = -u^r\left[2\sqrt{\frac{\omega^2E_0h^2}{3\rho_0(1-\nu^2)}}\frac{\nabla^2 e}{\eta_0\omega} - \eta_0\omega e\right]. \tag{57}$$

Thus, the resulting system matrix $\mathbf{K}$ is dependent upon u^r. Eq. (56) can be expressed in terms of the design variable $\mathbf{u}$ as

$$\frac{d^2\Pi}{du_i^2} = \left(\frac{\partial\mathbf{t}}{\partial u_i}\right)^T\mathbf{K}^{-1}\left(\frac{\partial\mathbf{t}}{\partial u_i}\right) - \frac{1}{2}r(r-1)\delta_{ij}\mathbf{e}^T\tilde{\mathbf{K}}(u_j^{(r-2)})\mathbf{e}, \tag{58}$$

where $\tilde{\mathbf{K}}$ is the second-order derivative of the system matrix $\mathbf{K}$ with respect to the design variable $\mathbf{u}$. If the penalty parameter "r" is equal to zero or one, the second term in Eq. (58) vanishes so that the problem is convex. Otherwise, it may have many local minima.

5. Numerical examples

5.1. Example 1: verification of sensitivity of energy density

The objective of this example is to verify the accuracy of the DSA method in energy density field. Note that all the examples from now on show the flexural wave cases not in-plane ones. Consider a rectangular plane structure that is 4 m long, 1 m wide, and 0.01 m thick. The structure is modeled using four node plate elements and subjected to the prescribed loading and boundary conditions on its bottom and top sides as shown in Fig. 2. The material properties are Young's modulus of $E = 195 \times 10^9$ (N/m^2), density of

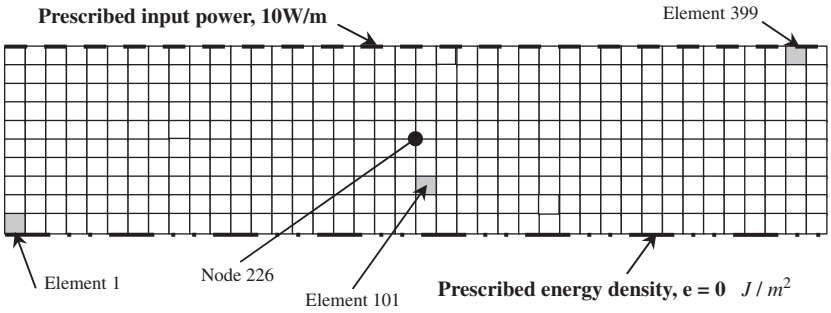

Fig. 2. Rectangular plate subjected to prescribed input power.

Fig. 3. Distribution of energy density e.

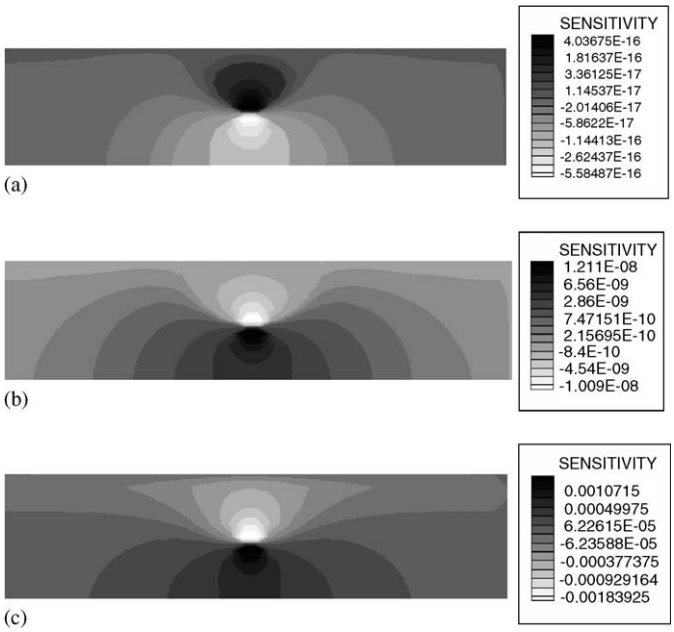

Fig. 4. Sensitivity of energy density at node 226 with respect to material properties: (a) young's modulus; (b) density; (c) damping factor.

$\rho = 7,800(\mathrm{kg/m^3})$, damping factor of $\eta = 0.01$, and Poisson's ratio of $v = 0.28$. Along the top side, the input power of 10 (W/m) with excitation frequency of 1000 Hz is applied. On the essential boundaries along the bottom side, the energy density of $e = 0$ is prescribed. The design variable and performance measure are selected as the material properties of each element and the energy density at node 226, respectively. For this model, the energy density is initially distributed as shown in Fig. 3.

The design sensitivity of energy density at node 226 with respect to the various material properties of each element is contoured in Fig. 4. The variation of Poisson's ratio is not considered during the optimization since

Table 1
Comparison of design sensitivity

Material property	Design variable	$\frac{de_{226}}{du_i}$	$\frac{\Delta e_{226}}{\Delta u_i}$	$\frac{de_{226}}{du_i} \Big/ \frac{\Delta e_{226}}{\Delta u_i}$ (%)
Young's modulus	E_1	−0.761054E-17	−0.761054E-17	100.00
	E_{101}	−0.214625E-15	−0.214625E-15	100.00
	E_{399}	−0.923153E-18	−0.923153E-18	100.00
Density	ρ_1	0.190263E-09	0.190256E-09	100.01
	ρ_{101}	0.536312E-08	0.536314E-08	100.00
	ρ_{399}	0.230908E-10	0.230908E-10	100.00
Damping factor	η_1	0.295777E-04	0.295777E-04	100.00
	η_{101}	0. 791392E-03	0. 791392E-03	100.00
	η_{399}	−0. 188783E-04	−0. 188783E-04	100.00

it is not significantly affecting the analysis results. For the elements around the node 226, the increase of Young's modulus results in the increase of the energy density. On the other hand, the increases of density and damping factor result in the decrease of the energy density.

The obtained analytical sensitivity is compared with the finite difference one. In Table 1, the sensitivity of energy density at node 226 with respect to the bulk material density of each element (u_i) is compared. de_{226}/du_i stands for the analytical sensitivity using either the DDM or the adjoint variable method (AVM). Those methods yield an identical result. $\Delta e_{226}/\Delta u_i$ represents the central finite difference sensitivity. The last column shows the percent agreement between the finite difference and the analytical sensitivities. Excellent agreements are observed everywhere.

In Table 2, the CPU costs required for the computation of design sensitivity are summarized. Only 0.078 s is required for the AVM and 10.9 s for the DDM whereas 55.125 s for the FDM. In general, the DDM requires approximately 19.77% of CPU time for the FDM. However, the AVM does only 0.15% of CPU time for the FDM. Comparing the DDM and AVM, the AVM just requires approximately 0.7% of CPU time necessary for the DDM.

5.2. Example 2: validation of topology optimization results

The purpose of topology optimization in the power flow problems is to find an optimal material layout that yields low energy density distribution in the structure under the prescribed loading and boundary conditions. In other words, the topology optimization helps to find a material layout hard to increase the energy density in the structure for the given input power and boundary conditions. The structure is modeled using four node plate elements and subjected to the prescribed loading and boundary conditions as shown in Fig. 5(a). The material properties are the same as the ones used in the previous example.

The topology design optimization is carried out under the constraint of allowable material volume of 40%, minimizing the generalized compliance. Vibrational power is coming into the middle of top side at the rate of 10 kW/m and out of both ends of bottom side at the rate of 1.4 kW/m. Regard the bulk material density of each element as the design variable and recall Eqs. (35) and (36) for the penalization of bulk material. Taking $p = 5$, $s = 1$, and $r = 1$, one obtains a linear variation of bulk material density u as

$$\begin{aligned}\pi &= -u^{(p-2r-s)/2} 2\sqrt{\frac{\omega^2 E_0 h^2}{3\rho_0(1-\nu^2)}}\frac{\nabla^2 e}{\eta_0\omega} + u^r \eta_0 \omega e \\ &= -u\left[2\sqrt{\frac{\omega^2 E_0 h^2}{3\rho_0(1-\nu^2)}}\frac{\nabla^2 e}{\eta_0\omega} + \eta_0\omega e\right].\end{aligned} \tag{59}$$

The optimal material distribution is shown in Fig. 5(b).

Table 2
Comparison of CPU time

FDM	DDM (DDM/FDM %)	AVM (AVM/FDM %)
55.12500	10.81250 (19.77%)	0.078125 (0.15%)

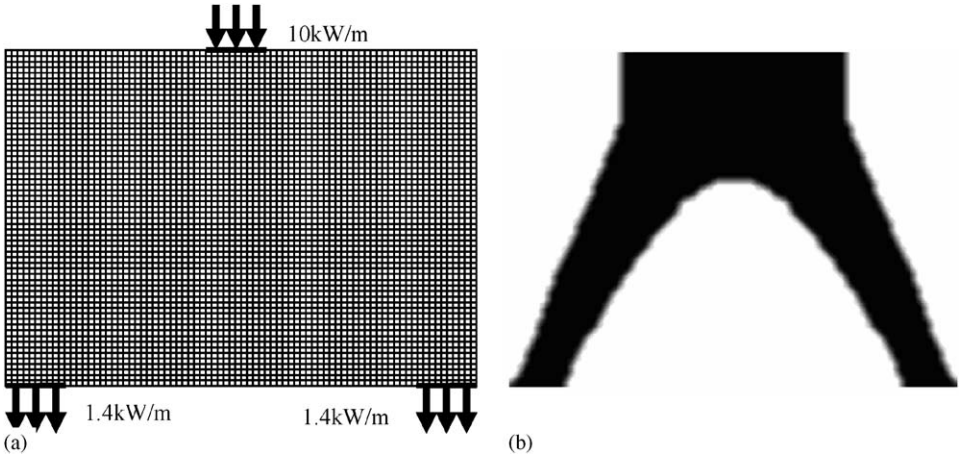

Fig. 5. Models for validation of topology optimization results: (a) before optimization and (b) after optimization.

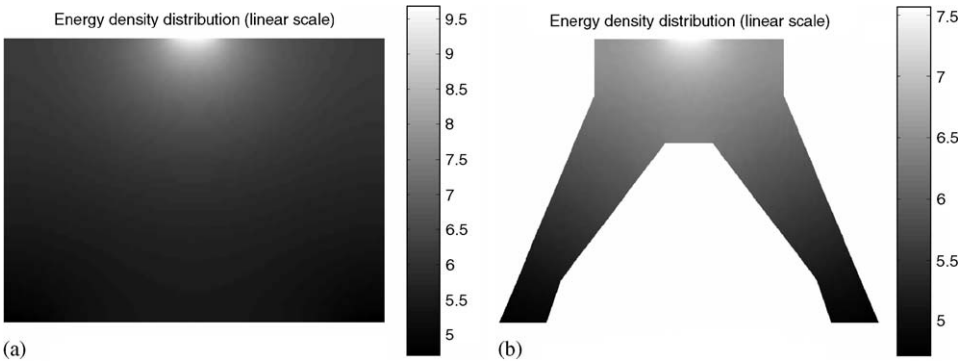

Fig. 6. Comparison of energy density distributions: (a) before optimization and (b) after optimization.

5.2.1. Distribution of energy density

To validate the effectiveness of topology optimization, two models at the excitation frequency of 1000 Hz are prepared. The one has uniformly distributed material properties whose magnitudes are reduced by 40% of the original ones, as shown in Fig. 6(a). The other is the one obtained after the topology optimization shown in Fig. 6(b), which keeps the original material properties. The model in Fig. 6(b) is constructed, based on the optimization result, removing the void region of the original model to meet the volume constraint, 40% of the original material volume.

In Fig. 6, the distributions of energy density in the models are compared. As expected, the optimal model (b) yields low energy density distribution throughout the whole domain, using an identical amount of material. The energy density distributions are approximately $4.71\sim9.68\,J/m^2$ for the model (a) and $4.72\sim7.57J/m^2$ for the model (b). The optimal result shows that the energy density is evenly distributed and its maximum is reduced by 22%.

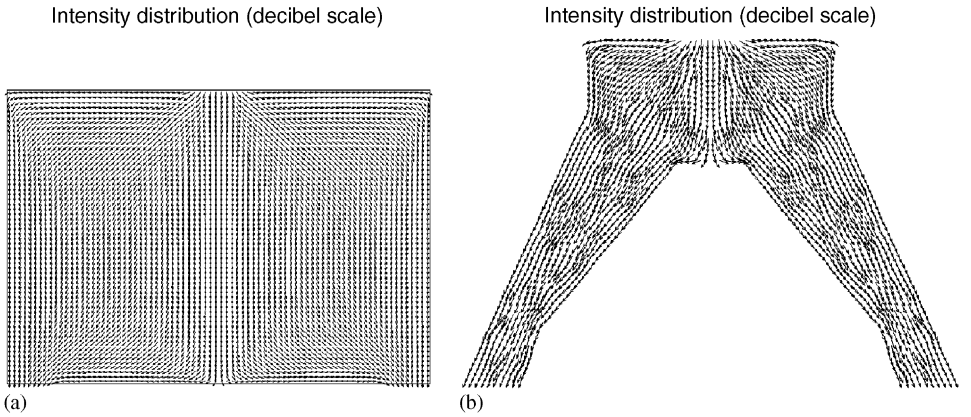

Fig. 7. Comparison of intensity distributions: (a) before optimization and (b) after optimization.

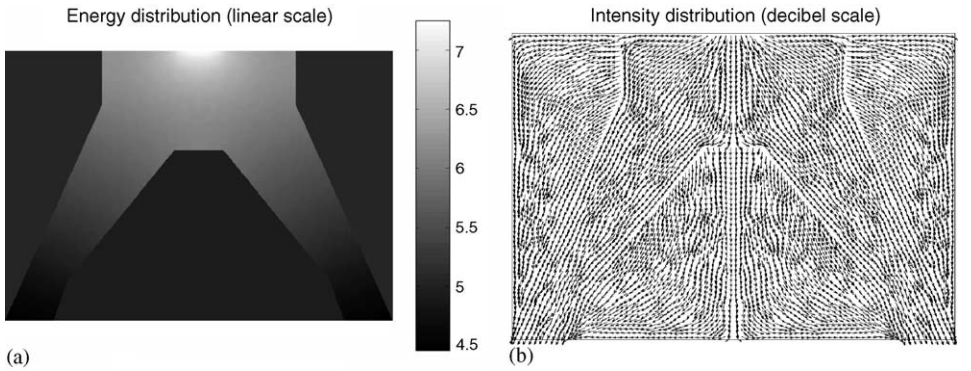

Fig. 8. Optimal design with void region and interface: (a) energy density and (b) intensity.

5.2.2. Distribution of intensity

The intensity distributions are compared in Fig. 7. The intensity **I** is defined as a vector that indicates the propagation direction of time-and space-averaged energy density flow. Comparing the intensity in the original model (a) with that in the optimal model (b), the optimization process is performed in such a way that the regions of less intensity are removed.

5.2.3. Validation of optimal design

To validate the topology optimization method, two models are considered. One is the optimal model with the void regions removed, as shown in Fig. 5(b). The other is the optimal model without the void regions removed. The void regions have less than 1% of the original bulk material density. Interface conditions between the void and solid regions are considered in this example. The boundary conditions using diffuse power transmission and reflection coefficients are used between void and solid regions [9]. The optimal model without void regions has the distribution of energy density ranging $4.72\sim7.57\,\mathrm{J/m^2}$ whereas the optimal model with void regions $4.67\sim7.47\,\mathrm{J/m^2}$. The difference is only $1.1\sim1.3\%$ so that the material layout obtained from the topology optimization can provide useful information for the layout design of structural systems (Fig. 8).

5.3. Example 3: topology optimization of rectangular plates

The design domain, boundary and loading conditions for three models using four node plate elements are illustrated in Fig. 9. Material properties, design variables, penalty parameters, and allowable volume fraction

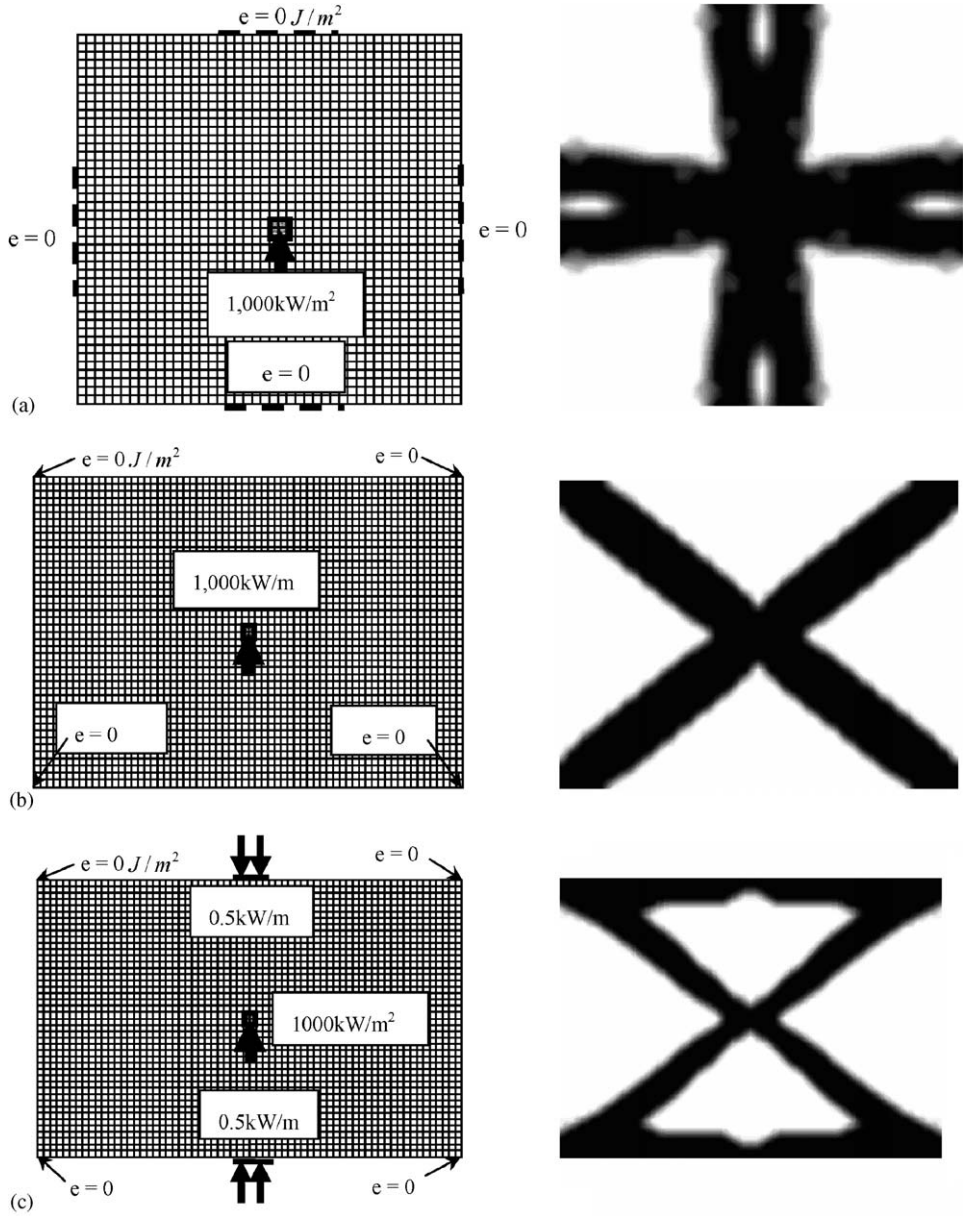

Fig. 9. Topology optimization with various loading and boundary conditions: (a) model A; (b) model B; (c) model C.

Table 3
Comparison of optimization cost

	Model A	Model B	Model C
Number of iterations	99	172	175
Number of sensitivity evaluations	10	14	14
CPU time (s)	248.40	1739.8593	1527.56

are the same as the ones used in the previous examples. The final material distributions after the topology optimization are shown in Fig. 9 as well. For model A, an input power π of 1000 kW/m^2 is applied at the center of model and the prescribed energy density conditions are imposed at the middle of four sides. For

model B, different boundary conditions are imposed. For model C, additional loadings are applied at the middle of top and bottom sides. Through numerical examples, one can notice that the optimal material layout requires a shortest distance between the loading and boundary to effectively release the stored energy density. In Table 3, the computational costs required for the models are compared. The topology optimization uses the modified method of feasible direction algorithm and requires 10–14 sensitivity evaluations. The CPU cost for the whole optimization process takes less than 1 h on a Pentium IV personal computer as shown in Table 3.

6. Conclusions

Weak formulation for the power flow problems in steady state is derived and continuum-based DSA methods are developed in both direct differentiation and adjoint approaches. Also, a topology design optimization method for the power flow problems is developed utilizing the adjoint DSA method. Since the already factorized tangent matrix is utilized in the adjoint method, the computing cost is trivial compared with the finite difference method. For the topology design optimization, the design variables of material properties are parameterized using a bulk material density function. Through numerical examples, the accuracy and efficiency of the DSA method are verified by comparing with the finite difference sensitivity. Comparing the efficiency of developed method, it just requires only 0.15% of CPU cost for the finite difference method. Comparing the energy density distributions before and after the topology optimization, significantly reduced energy density distribution is observed everywhere. The material layout obtained from the topology optimization can provide useful information for the layout design of structural systems.

Acknowledgement

This work was supported by Advanced Ship Engineering Research Center of the Korea Science and Engineering Foundation (Grant number R11-2002-104-06003-0, R11-2002-104-09002-0) in 2005–2006. The support is gratefully acknowledged.

References

[1] V.D. Belov, S.A. Rybak, B.D. Tartakovskii, Propagation of vibrational energy in absorbing structures, *Journal of Soviet Physics Acoustics* 23 (2) (1977) 115–119.
[2] I.A. Butlitskaya, A.I. Vyalyshev, B.D. Tartakovskii, Propagation of vibrational and acoustic energy along a structure with losses, *Journal of Soviet Physics Acoustics* 29 (4) (1983) 333–334.
[3] L. Cremer, M. Heckl, E.E. Ungar, *Structure-Borne Sound*, Springer, Berlin, 1988.
[4] D.J. Nefske, S.H. Sung, Power flow finite element analysis of dynamic systems: Basic theory and application to beams, *Journal of Vibration, Acoustics, Stress and Reliability in Design* 111 (1989) 94–100.
[5] Y. Lase, L. Jezequel, Analysis of a dynamic system based on a new energetic formulation, *International Congress on Intensity Techniques*, Senlis, France, 1990, pp. 145–150.
[6] O.M. Bouthier, R.J. Bernhard, Simple models of the energy flow in vibrating membranes, *Journal of Sound and Vibration* 182 (1) (1995) 129–147.
[7] O.M. Bouthier, R.J. Bernhard, Simple models of the energetics of transversely vibrating plates, *Journal of Sound and Vibration* 182 (1) (1995) 149–166.
[8] P.E. Cho, *Energy Flow Analysis of Coupled Structures, PhD Thesis*, Purdue University, West Lafayette, IN, 1993.
[9] D.H. Park, S.Y. Hong, H.G. Kil, J.J. Jeon, Power flow models and analysis of in-plane waves in finite coupled thin plates, *Journal of Sound and Vibration* 244 (4) (2001) 651–668.
[10] M.P. Bendsøe, N. Kikuchi, Generating optimal topologies in structural design using a homogenization method, *Computer Methods in Applied Mechanics and Engineering* 71 (1988) 197–224.
[11] M.P. Bendsøe, Optimal shape design as a material distribution problem, *Structural Optimization* 1 (1989) 193–202.
[12] Q. Li, G.P. Steven, O.M. Querin, Y.M. Xie, Shape and topology design for heat conduction by evolutionary structural optimization, *International Journal of Heat and Mass Transfer* 42 (1999) 3361–3371.
[13] E.J. Haug, K.K. Choi, V. Komkov, *Design Sensitivity Analysis of Structural Systems*, Academic Press, New York, 1986 pp. 83–109.
[14] N.H. Kim, J. Dong, K.K. Choi, Energy flow analysis and design sensitivity analysis of structural problems at high frequencies, *Journal of Sound and Vibration* 269 (2004) 213–250.
[15] D.A. Tortorelli, R.B. Haber, Stephen C-Y. Lu, Design sensitivity analysis for nonlinear thermal systems, *Computer Methods in Applied Mechanics and Engineering* 77 (1989) 61–77.

[16] D.A. Tortorelli, R.B. Haber, First-order design sensitivity analysis for transient conduction problems by an adjoint method, *International Journal for Numerical Methods in Engineering* 28 (1989) 733–752.
[17] A. Sluzalec, M. Kleiber, Shape sensitivity analysis for nonlinear steady-state heat conduction problems, *International Journal of Heat and Mass Transfer* 39 (1996) 2609–2613.